DNS OF TURBULENT CHANNEL FLOW AT VERY LOW REYNOLDS NUMBERS

Takahiro Tsukahara, Yohji Seki, Hiroshi Kawamura
Department of Mechanical Engineering,
Tokyo University of Science
Yamazaki 2641, Noda-shi, Chiba 278-8510, Japan
a7599109@rs.noda.tus.ac.jp, a7598074@rs.noda.tus.ac.jp, kawa@rs.noda.tus.ac.jp

Daisuke Tochio
Department of HTTR Project,
Oarai Research Establishment,
Japan Atomic Energy Research Institute
Oarai-machi, Higashiibaraki-gun, Ibaraki 311-1394, Japan
tochio@oarai.jaeri.go.jp

ABSTRACT

Direct numerical simulation (DNS) of a fully developed turbulent channel flow for very low Reynods numbers has been executed with larger computational box-sizes than those of common DNS. The present Reynolds number is decreased down to $Re_\tau = 64$, where Re_τ is based on the friction velocity and the channel half width δ. For Re_τ=80 with using the largest box of $51.2\delta \times 2\delta \times 22.5\delta$, the periodic weak-turbulence regions are observed. This type of locally disordered flow is similar to a turbulent puff observed in a transitional pipe flow. Various turbulence statistics such as turbulent intensities, vorticity fluctuations, Reynolds stresses are provided. Especially, their near-wall asymptotic behavior and budget terms of turbulence kinetic energy are obtained and discussed with respect to Reynolds number dependence and an influence of the comptational box-size. In addition, two-point correlation coefficients, visualized instantaneous flow fields and the pre-multiplied energy spectra are presented in order to examine turbulence structures.

INTRODUCTION

A low Reynolds number flow in a channel is of practical importance with respect to a high temperature gas-cooled nuclear reactor, in which the low Reynolds number is employed to obtain a high outlet gas temperature. Direct numerical simulations (DNS, hereafter) of a fully developed turbulent channel flow have been increasingly performed for higher Reynolds numbers with an aid of recent development of computers. A DNS provides various information, such as velocity and pressure. Special attention has been paid to their near-wall asymptotic behavior and their derivatives at any time and point in the instantaneous field, which are extremely difficult to be measured in experiments.

The first DNS of the fully developed turbulent channel flow was made by Kim *et al.* (1987). Their Reynolds number was Re_τ=180, which is based on the channel half width δ, the kinematic viscosity ν and the friction velocity $u_\tau = \sqrt{\tau_w/\rho}$, where τ_w is the statistically averaged wall shear stress and ρ is the density. Kuroda *et al.* (1989) carried out the DNS for a slightly lower Reynolds number of Re_τ=150. The author's group (Kawamura *et al.*, 1998; Abe *et al.*, 2004a, 2004b) performed the DNS with respect to Reynolds number and Prandtl number dependences for Re_τ=180-1020. As for the low Reynolds number, several research groups carried out the DNS down to Re_τ=80 in order to study a control of turbulence (Bewley *et al.*, 2001; Chang *et al.*, 2002; Högberg *et al.*, 2003). Iwamoto *et al.* (2002) have executed the DNS for Re_τ=110-650; their published results of Re_τ=110 and 150 are also included in this paper for comparison. These studies often employed rather small computational boxes because of limited calculation resources. A great deal of effort has been conducted to experimental studies of the turbulent channel flow. Laufer (1951) first obtained the detailed turbulence statistics in the channel flow. Patel and Head (1969) measured skin friction and mean velocity profiles over the Re_m range 1,000-10,000 that includes the transition from laminar to turbulent flow, where Re_m based on the bulk mean velocity u_m and the channel width. Later, Kreplin and Eckelmann (1979) made their experiments for low Reynolds numbers of Re_c=2,800-3,850, based on the centerline velocity u_c and δ. The measurements of the turbulent channel flow at Re_c=2,850 or 3,220 were executed by Niederschulte *et al.* (1990).

Table 1: Reynolds numbers of the present DNS; i.e., $Re_\tau=u_\tau\delta/\nu$, $Re_m=u_m 2\delta/\nu$, $Re_c=u_c\delta/\nu$. MB, medium box-size; SB, semi-large box-size; LB, large box-size, cf., Table 2.

Re_τ	180	150	110	80	80	70	64
Re_m	5730	4620	3290	2290	2320	2020	1860
Re_c	3360	2720	1960	1400	1430	1270	1200
Box size	MB	MB	MB	MB	LB	SB	SB

Recently, much attention is paid to a large-scale structure (LSS) in the turbulent channel flow (Jiménez, 1998; Liu *et al.*, 2001; Abe *et al.*, 2004a, 2004b). For the lower Reynolds number, the near-wall streak structure is so elongated that its length exceeds the usual computational box-size. Thus DNS of the low Reynolds number flow requires a larger box-size to capture the near-wall streak structure and the LSS.

In the present work, the DNS of fully developed turbulent channel flow has been carried out with the use of larger computational boxes than existing works. The purpose of this study is to obtain the turbulence statistics and characteristics of the turbulent channel flow at the very low Reynolds numbers.

Table 2: Computational domain size; L_i, N_i and Δi are a box length, a grid number and a spatial resolution of i-direction.

Box size	MB	SB	LB
L_x^*, L_z^*	12.8, 6.4	25.6, 12.8	51.2, 22.5
N_x, N_z	256, 256	256, 256	1024, 512
N_y	128	128	96
$\Delta x^*, \Delta z^*$	0.05, 0.025	0.10, 0.05	0.05, 0.044
$\Delta y^*_{\mathrm{min,max}}$	0.0011-0.033	0.0011-0.033	0.0014-0.045

NUMERICAL PROCEDURE

The mean flow is driven by the uniform pressure gradient. It is assumed to be fully developed in streamwise (x-) and spanwize (z-) directions. The coordinates and the flow variables are normalized by u_τ, ν and δ. Periodic conditons are imposed in the x- and z- directions and the nonslip is applied on the walls. The fundamental equations are the continuity and the Navier-Stokes equations. For the spatial discretization, the finite difference method is adopted. The numerical scheme with the 4th-order accuracy is employed in the streamwise and spanwize directions, while the one with the 2nd-order is applied in the wall-normal direction. Time advancement is executed by the semi-implicit scheme: the 2nd-order Crank-Nicolson for the viscous terms (wall-normal direction) and the 2nd-order Adams-Bashforth methods for the other terms.

In the present work, a series of DNS has been made for Re_τ=64-180 (see Table 1). For the lower Reynolds numbers of Re_τ=64-80, the larger boxes than those of common DNS are adopted. The computational conditions are shown in Table 2. The nonuniform meshes are applied in the wall-normal direction. Note that quantities with the superscript of * indicate those normalized by the outer variables, e.g., $y^* = y/\delta$. In the present DNS, the pressure gradient is decreased stepwisely down to an estimated level for the aimed Reynolds number. The fully developed flow field at higher Reynolds number is successively used as the initial condition for the one-step lower Reynolds number, e.g., Re_τ=180→150, 150→110, 110→80 and so on. Note that various statistical data are obtained after the flow has reached a statistical-steady state.

RESULTS AND DISCUSSION

Mean velocity profile

Figure 1 shows the vertical profile of the dimensionless mean velocity in wall units, where quantities with the superscript of $^+$ indicate those normalized by the wall variables, e.g., $y^+ = yu_\tau/\nu$. Statistics are denoted by a overline of $\overline{(\,)}$, that are the spatial (in the horizontal directions) and temporal averaging. The obtained data from the experiments of Patel and Head (1969) and the DNS by Iwamoto *et al.* (2002) using the spectral method are also shown for comparison. The present results for Re_τ=110-180 are in good agreement with the DNS of Iwamoto *et al.*. In these low Reynolds number flows, the mean velocity distributions do not indicate the logarithmic region clearly. For the lower Reynolds numbers of $Re_\tau \leq 110$, von Kármán constant (not shown here) does not exhibit any constant range at all. In the outer region ($y^+ > 10$), a significant Reynolds number dependence is found when normalized by the inner variables. Mean flow variables such as the bulk mean velocity $\overline{u}_m^+$ and the mean centerline velocity $\overline{u}_c^+$ are

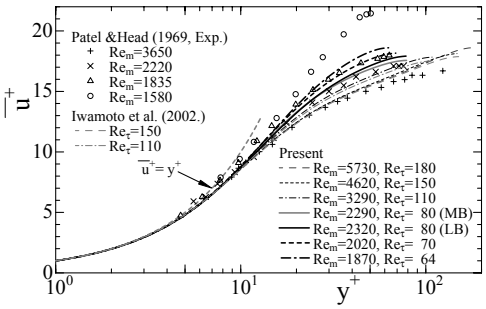

Figure 1: Mean velocity profile in viscous wall units

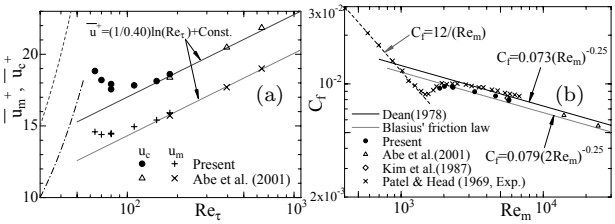

Figure 2: Reynolds number *versus* (a) centerline velocity u_c^+ and bulk mean velocity u_m^+, (b) friction coefficient C_f. In (a), dotted lines (– – – –, — · —) show the laminar flow relations of $u_c = Re_\tau/2$ and $u_m = Re_\tau/3$, respectively.

given in Fig. 2(a) for each Reynolds number. It is interesting to note that the values of $\overline{u}_c^+$ and $\overline{u}_m^+$ increases with decreasing Reynolds number, if Re_τ <80. The reason will be discussed later. Both $\overline{u}_c^+$ and $\overline{u}_m^+$ are expected to approach gradually to laminar values.

Although the skin friction coefficient is one of the most fundamental turbulence characteristics, the one in the transitional region of the channel flow has not been examined yet through the DNS owing to the lack of the low Reynolds number simulations. Figure 2(b) shows a variation of the skin friction coefficient C_f=$2\tau_w/(\rho \cdot u_m^2)$ in comparison with the empirical correlations proposed by Dean (1978) for a channel flow, and by Blasius for a pipe flow. The present results are in good agreement with them for $Re_m > 3000$. It is worth noting that, for $Re_m < 3000$, C_f tends to be smaller than the empirical correlations with the decreasing Reynolds number, and it agrees well with the experimental data from Patel and Head (1969). It is found that the present Reynolds number is close to the laminarization. The lowest Reynolds number of Re_m =1860 in the present DNS lays still in the transitional region. The lower limit cannot be clealy defined by the calculation up to now.

Turbulence intensity

The root-mean-square (r.m.s.) of the streamwise velocity fluctuation normalized by u_τ is given in Fig. 3. If u'^+_{rms} is plotted against y/δ, it increases remarkably in the central region of the channel for $Re_\tau < 80$. The value of the local maximum near the wall decreases remarkably at $Re_\tau \leq 70$.

With respect to the computational box-size, a significant influence of the box-size upon u'^+_{rms} can be seen for Re_τ=80 at the central region. With extending box size, u'^+_{rms} is enhanced, with a deviation of about 12% at the channel center. This is because the turbulence structure is confined by a short box length in the case of Re_τ=80(MB). This tendency is also

Table 3: Near-wall expansion coefficient

Re_τ	b_1	c_2	b_3	$\overline{b_1 c_2}$
180	0.360	8.70×10^{-3}	0.189	7.30×10^{-4}
180†	0.356	8.5×10^{-3}	0.190	7.0×10^{-4}
150	0.354	8.60×10^{-3}	0.172	7.10×10^{-4}
110	0.336	6.75×10^{-3}	0.145	5.45×10^{-4}
80(MB)	0.302	4.55×10^{-3}	0.105	3.45×10^{-4}
80(LB)	0.333	6.85×10^{-3}	0.144	4.45×10^{-4}
70	0.291	4.65×10^{-3}	0.101	3.10×10^{-4}
64	0.268	3.90×10^{-3}	0.086	2.45×10^{-4}

† Antonia and Kim (1994)

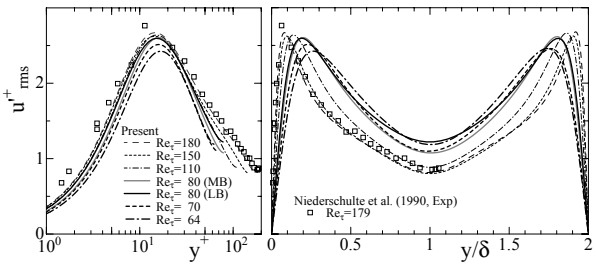

Figure 3: R.m.s. of the streamwise velocity fluctuation u'

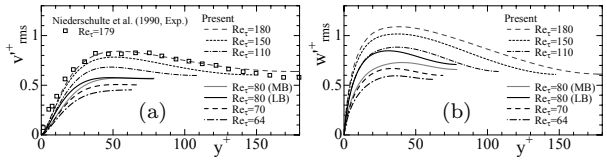

Figure 4: R.m.s. of the wall-normal fluctuation v' (a) and the spanwise fluctuation w' (b).

seen for spanwise fluctuations in the whole channel (Fig. 4(b)), with a deviation of 7-27%. The influence upon the wall-normal component is small (Fig. 4(a)). Moreover, the influence of the box-size on the mean flow variables and other turbulence quantities, such as $\overline{u}^+$, vorticity fluctuations (shown later), are also significant at very low Reynolds number of Re_τ=80, whereas the those of the box-size on the tubulence statistics are rather small for the moderate Reynolds number of Re_τ=180-640 as shown by Abe *et al.* (2004a).

Effect of Reynolds number is significant in the $u_{i\,\mathrm{rms}}'^+$ of both spanwise and wall-normal directions. All component values decrease with the decrease of Reynolds number. Antonia *et al.* (1992) indicated that the Reynolds number dependence of $w_{\mathrm{rms}}'^+$ is more significant compared to that of $u_{\mathrm{rms}}'^+$ and $v_{\mathrm{rms}}'^+$. In the present work, both $v_{\mathrm{rms}}'^+$ and $w_{\mathrm{rms}}'^+$ decrease remarkably with the decreasing Re_τ. This is because the production term of $u_{\mathrm{rms}}'^+$ and redistribution for $v_{\mathrm{rms}}'^+$ and $w_{\mathrm{rms}}'^+$ are reduced with the decreasing Re_τ as discussed later.

To analyse the near-wall asymptotic behaviour, the velocity fluctuations can be expanded in Taylor series about-the-wall value as follows:

$$\begin{cases} u'^+ = b_1 y^+ + c_1 y^{+2} + \cdots \\ v'^+ = \qquad\quad c_2 y^{+2} + \cdots \\ w'^+ = b_3 y^+ + c_3 y^{+2} + \cdots . \end{cases} \tag{1}$$

The r.m.s. values of the vorticity fluctuations are shown in Fig. 5. The streamwise and spanwise vorticity fluctuations, $\omega_x'^+(=b_3)$ and $\omega_z'^+(=b_1)$, decrease with decreasing

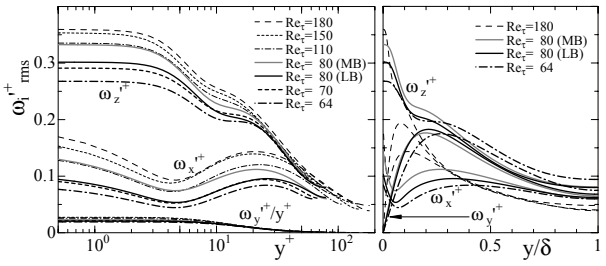

Figure 5: R.m.s. of vorticity fluctuation

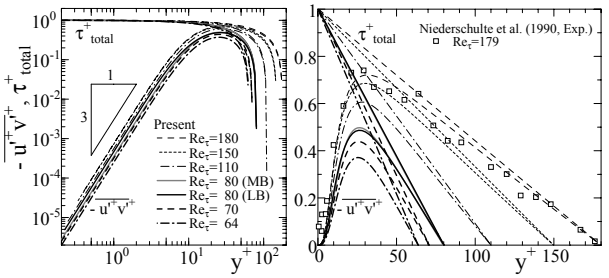

Figure 6: Reynolds shear stress and total shear distribution

Reynolds number. However, the influence of insufficient box size for Re_τ=110 and 80(MB) cannot be neglected. The ratio $\omega_y'^+/y^+(=b_{1,3}-b_{3,1})$ tends to become constant in the near-wall region as reported by Antonia and Kim (1994).

The use of Eq. (1) in the expression for the Reynolds shear stress, $-\overline{u'^+v'^+}$, yields

$$-\overline{u'^+v'^+} = -\overline{b_1 c_2} y^{+3} + \cdots . \tag{2}$$

The near-wall values of b_1, c_2, b_3 and $\overline{b_1 c_2}$ are extrapolated up to the wall, and are given in Table 3. The present result of Re_τ=180 agrees well with that of Antonia and Kim (1994). These coefficients decrease with the decrease of Reynolds number. This is because the production rate of the turbulent kinetic energy decreases with decreasing Reynolds number as discussed later. Especially, the decrease of c_2, b_3 and $\overline{b_1 c_2}$ is significant when the Reynolds number falls to 70; the decrease in $\overline{b_1 c_2}$ is slightly larger than that for either c_2 or b_3. In the case of $Re_\tau \leq 80$(MB), however, the obtained coefficients could be furtherl influenced by the box-size.

Reynolds shear stress

Figure 6 shows the Reynolds shear stress $-\overline{u'^+v'^+}$ and the total shear stress τ_{total}. As the Reynolds number decreases, the peak value of $-\overline{u'^+v'^+}$ decreases and its position moves close to the wall, if scaled with the wall unit. When Re_τ is 180, the peak of $-\overline{u'^+v'^+}$ reaches 0.72 at y^+=32, while, in the case of Re_τ=64, it becomes 0.37 at y^+=26.

In the fully depeloped channel flow, the production term of the turbulent kinetic energy is expressed as

$$P_k = -\overline{u'^+v'^+}\frac{\partial \overline{u}^+}{\partial y^+} = -\overline{u'^+v'^+}\left[1 - \frac{y^+}{Re_\tau} - \left(-\overline{u'^+v'^+}\right)\right]. \tag{3}$$

Thus the peak value of P_k can be calculated as

$$P_k = \frac{1}{4}\left[1 - \frac{y^+_{\max}}{Re_\tau}\right]^2 \text{ at } \left\{ y^+ \middle| -\overline{u'^+v'^+} = \frac{\partial \overline{u}^+}{\partial y^+} \right\}. \tag{4}$$

Here, the wall-normal position of the peak of P_k is denoted as $y^+_{\max}$, where the Reynolds shear stress and the viscos stress

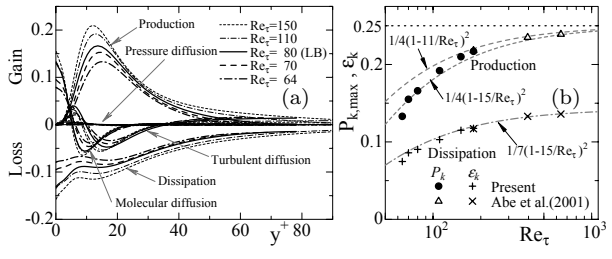

Figure 7: Budget of turbulent kinetic energy k normalized by ν/u_τ^4; (b) variation of the peak of production term $P_{k,\max}$ and the dissipation rate ε_k at the same height.

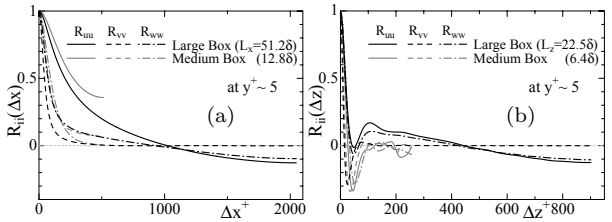

Figure 8: Two-point correlation coefficients R_{ii} of the velocity fluctuation component at $Re_\tau = 80$; (a) streamwise, (b) spanwise.

are equal to half of the total shear stress. In the present calculation, $y^+_{\max}$ is 11 for Re_τ=180; while, decreasing Reynolds number, it moves away from the wall and reaches at $y^+_{\max} \approx$15 for $Re_\tau \approx 15$. In addition, this indicates that the peak value of P_k decreases with decreasing Re_τ (see Fig. 7(a)). Figure 7(b) shows the peak value of P_k and dissipation rate ε_k at $y^+_{\max}$ for each Reynolds number. The decrease in $P_{k,\max}$ with decreasing Re_τ is clearly more prominent than that of ε_k. This is the reason why the turbulent intensities are decreased in the near-wall region with the decreasing Re_τ, as seen in Figs. 3 and 4 and in Table 3.

Turbulence structure: instantaneous flow fields

The effect of the box size can be most clearly observed in the streamwise and spanwise two-point correlations of velocity fluctuation R_{ii}, which is shown in Fig. 8. For Re_τ =80(MB), R_{uu} does not fall down to zero, indicating that the box-size is not large enough; especially, the streamwise box length is too short to contain the streak structures in the near-wall region (Fig. 8(a)). On the other hand, R_{uu} and R_{ww} fall down to negative values at the mid box-length for both stream- and the spanwise directions for the large box-size (LB), while R_{vv} falls off to almost zero. It points out that one long wavelength structure is captured with this large box (LB). In addition, a significant decrease in the magnitude of the negative maximum is found at the spanwise separation distance of $z^+ \approx 50$ which corresponds to the spanwise spacing of the near-wall streak structures (Fig. 8(b)). These suggest that there exists an influence of the LSS not only in the channel center but also in the near-wall region. The spacing of the streak structures and the LSS has been investigated with the use of the pre-multiplied energy spectra, which will be discussed later.

The streamwise and spanwise pre-multiplied energy spectra for Re_τ =80 are shown in Fig. 9 with reference to Jiménez (1998). The peak position of the pre-multiplied energy spectra gives the most energetic wavelength (MEW). It is in-

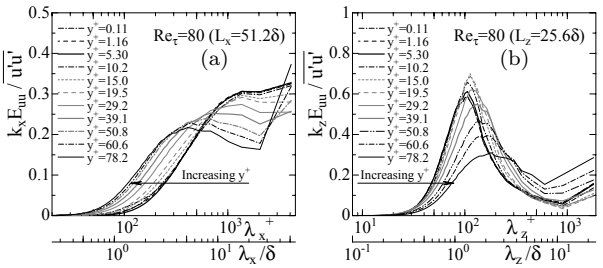

Figure 9: Pre-mulitplied energy spectra for $Re_\tau = 80$; (a) $k_x E_{uu}/\overline{u'u'}$, (b) $k_z E_{uu}/\overline{u'u'}$.

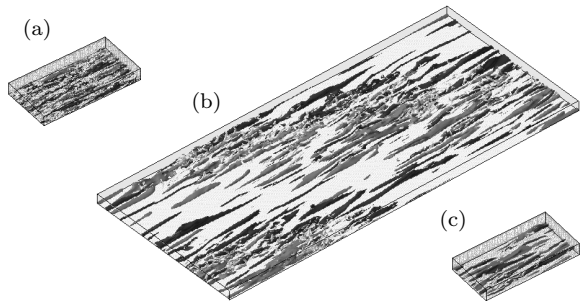

Figure 10: Instantaneous flow fields; high (gray) and low (dark-gray) speed regions of u'^+ and negative regions (light-gray) of the second invariant of deformation tensor $u'_{i,j}u'_{j,i}$. (a) Re_τ =180, (b) Re_τ =80(LB), (c) Re_τ =80(MB). All of the box-size (a)-(c) are scaled by δ. Direction of the mean flow is from bottom-left to top-right.

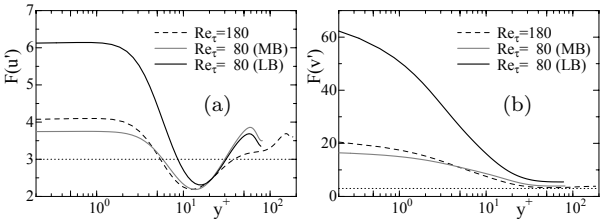

Figure 11: Flatness factor of velocity fluctuation; (a) streamwise component $F(u')$, (b) wall-normal component $F(v')$.

teresting to note that MEW in the wall vicinity stays still at about $\lambda_z^+ \approx$100 and not much changed from that of the higher Reynolds numbers even though the Re_τ is as low as 80 (Fig. 9(b)). Moving away from the wall, the MEW shifts slightly to the longer wavelengths. In the central region, on the other hand, a peak of MEW arises at about λ_z^+=180. This MEW corresponds to about 2.3δ, which shows a significant deviation from 1.3-1.6δ obtained for the higher Reynolds numbers, cf., Abe *et al.* (2004a). The streamwise MEW arises at $\lambda_x^+ \approx 1,000$ in the near-wall region. With increase in the distance from the wall, the streamwise MEW moves towards the shorter wavelength of $\lambda_x^+ \approx$500 (Fig. 9(a)). On the other hand, in the both directions, another peak appears at the longest wavelength in the core region, which corresponds to long-wavelength structures in the visualized flow field (Fig. 10(b)).

Figure 10 shows the high- and low-speed regions and the second invariant of deformation tensor ($II'=\partial u'_i/\partial x_j \times \partial u'_j/\partial x_i$) at Re_τ=180, 80(MB) and 80(LB). For Re_τ=180, the high- and low-speed streaks are evenly distributed as seen

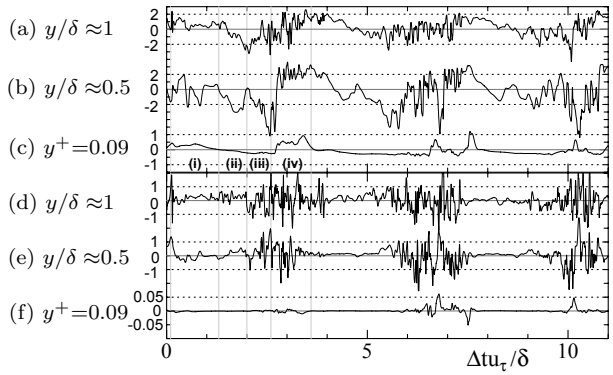

Figure 12: Typical time trace of u- and v-fluctuations at Re_τ=80(LB). The measurement points are at various wall-normal locations at the same position in the (x, z)-plane. (a)-(c), the streamwise fluctuation u'^+; (d)-(f), the wall-normal fluctuation v'^+.

in Fig. 10(a). For Re_τ=80(LB), on the contrary, the near-wall streaks are unevenly distributed and the sparse region can be observed. The shape of this flow field is so similar to that of the natural turbulent spot observed in experiments of the plane channel flow in transitional region, cf., Carlson *et al.*(1982). The well-known vortex structures such as quasi-streamwise vortices are unevenly distributed near the wall. In addition, these vortices are associated closely with the crowded near-wall streaks. The long-wavelength structure of the weak-turbulent (laminar-like velocity profile) region occurs periodicaly. Its streamwise wavelength occupies almost the whole box-length. This is a reason why the streamwise two-point correlations R_{uu} fall down to a negative value at the middle of the box as seen in Fig. 8.

The flatness factor of the velocity fluctuation is shown in Fig. 11. For Re_τ=80, comparison of the results with different box sizes indicates that the influence of box size upon the flatness factor is very significant (see 80(MB) and 80(LB)). If the box size is extended large enough to capture the highly disordered turbulent region and weak-turbulent regions, intermittency of fluctuation is enhanced. Moreover, an increase of the flatness factor with decreasing Reynolds number is found in the near-wall region.

Turbulence structure: puff-like structures

Wygnanski and co-workers (1973, 1975) conducted a study of the structures and phenomena associated with transitional and turbulent *pipe flow* in the range of $1,000 < Re_m < 50,000$. They identified two transitional flow states, the type observed being dependent on Re_m. For $2,000 < Re_m < 2,700$ the transition sturctures were termed 'turbulent puffs'; the second state is found at $Re_m > 3,500$ and consists of structures termed 'turbulent slugs'. Both a puff and a slug are characterized by a distinct trailing edge over which the flow changes almost discontinuously from turbulent flow to laminar flow. In the *channel flow* of the present study, the computational results shown in Fig. 12 are strikingly similar to experimental velocity traces obtained by Wygnanski and Champagne (1973) for a *pipe flow*. It is observed that the sequence of events as the structure is advected past the measurement point. It can be interpreted as: (i) laminar-like flow, (ii) a gradual reduction of u, (iii) a highly disordered turbulent region, (iv) a sharp interface with laminar-like flow, again return to (i) laminar-like flow. The intensities of both u' and v' are enhanced periodically with interval of $\Delta tu_\tau/\delta \approx 3.5$, so the upstream interface was observed to travel at a speed close to the bulk mean velocity $u_m^+ \approx 14.5$. With respect to the present Reynolds number, i.e. Re_m=2320, the obtained structures of co-existing weak-turbulent region as discussed above are consistent with and remarkably similar to the 'turbulent puffs' obserbed in a *pipe flow*.

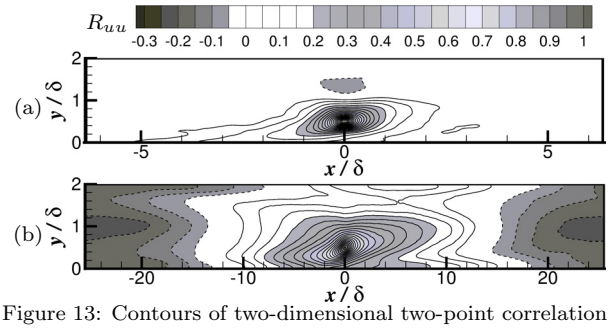

Figure 13: Contours of two-dimensional two-point correlation coefficient R_{uu} in the (x, y)-plane; the referece point is at the mid-height $y_{\rm ref} = 0.5\delta$. The direction of the mean flow is from left to right. (a) $Re_\tau = 180$; (b) $Re_\tau = 80$ (LB). ——, positive correlation; - - - -, negative correlation; the line of $R_{uu} = 0$ is not shown here. Contour interval ΔR_{uu}:0.05.

The shape of the structures in the wall-normal direction is clearly illustrated from the two-dimensional correlation for velocity in the (x, y)-plane. While the region of negative correlation appears in the side of the other wall for Re_τ=180 (Fig. 13(a)), the negative region appears in a wide region of $|\Delta x| > 13\delta$ for Re_τ=80(LB). This indicates that a puff-like structure with a large streamwise wavelength of $52h$ fills the entire channel width in the case of Re_τ=80(LB).

A typical well-developed structure at Re_τ=80(LB) is shown in the sequence of flow visualization presented in Fig. 14. The puff-like structure Fig. 14(a) are consist of a laminar-like flow (region A) and a highly disordered turbulence (region B). Figures 14(b)-(f) indicate that the stuctures are equilibrium and self-sustained. Moreover, the both regions propagate with the same streamwise velocity and are inclined at an angle of 24° with respect to the streamwise direction. Therefore, the puff-like structures are spatially distributed not only in streamwise but also spanwise, while the puff of a pipe flow is homogeneous in azimuthal and intermittent only in the streamwise direction. Note that the present results, such as visualized flow fields, two-point correlation (Fig. 8) and energy spectra (Fig. 9), show signs of being constrained by the periodicity of the boundary, even when the box-size was extended to $(L_x \times L_z)$=$(51.2\delta \times 22.5\delta)$; and the numerical box requires to be enlarged further.

CONCLUSIONS

In the present study, we performed DNS of the turbulent channel flow with larger computational boxes down to Re_τ=64 and investigated the turbulence statistics with respect to low Reynolds number effect.

- For $Re_m < 3000$ ($Re_\tau \leq 80$), C_f tends to be smaller than the empirical correlation. Reynolds number dependence of the mean velocity profile is significant in the outer region when scaled with the wall units.

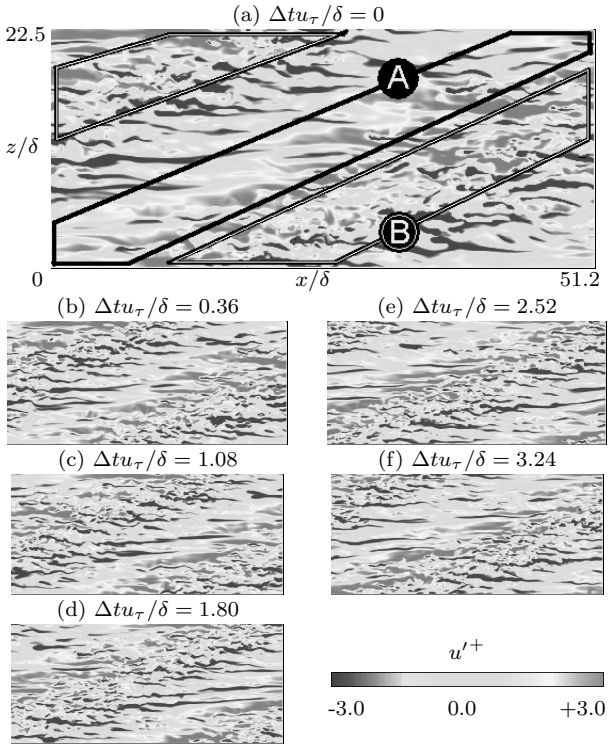

Figure 14: Contour of streamwise velocity fluctuation u'^+ for a series of consecutive times, in an (x, z)-plane at $y/\delta \approx 0.5$ for $Re_\tau = 80$ (LB). All of the contours (a)-(f) shows the whole (x, z)-plane of $L_x \times L_z = 51.2\delta \times 22.5\delta$. The direction of the mean flow is from left to right.

- For Re_τ=80, the periodic weak-turbulence region with the streamwise long-wavelength is observed with using the largest box of $51.2\delta \times 2\delta \times 22.5\delta$, and is very similar to a 'turbulent puff' observed in a transitional pipe flow.
- The significant effects of the captured puff-like structures exist upon the turbulence statistics, such as a mean velocity and turbulence intensities.
- The equilibrium puff-like structures observed in the channel flow inclines against the streamwise direction. The propagation velocity of the puff-like structure is approximately equal to the bulk mean velocity.

ACKNOWLEDGEMENTS

The present study is entrusted from Ministry of Education, Culture, Sports, Science and Technology of Japan. The present computations were performed with the use of VPP5000/64 at Computing and Communications Center of Kyushu University, and also supercomputing resources at Information Synergy Center of Tohoku University.

REFERENCES

Abe, H., Kawamura, H. and Choi, H., 2004a, "Very large-scale structures and their effects on the wall shear-stress fluctuations in a turbulent channel flow up to $Re_\tau = 640$", *Trans. ASME J. Fluids Eng.*, **126**, pp. 835-843.

Abe, H., Kawamura, H. and Matsuo, Y., 2004b, "Surface heat-flux fluctuations in a turbulent channel flow up to Re_τ=1020 with Pr=0.025 and 0.71", *Int. J. Heat and Fluid Flow*, **25**, pp. 404-419.

Antonia, R. A., Teitel, M., Kim, J. and Browne, L. W. B., 1992, "Low-Reynolds-number effects in a fully developed turbulent channel flow", *J. Fluid Mech.*, **236**, pp. 579-605.

Antonia, R. A. and Kim, J., 1994, "Low-Reynolds-number effects on near-wall turbulence", *J. Fluid Mech.*, **276**, pp. 61-80.

Bewley, T. R., Moin, P. and Temam, R., 2001, "DNS-based predictive control of turbulence: an optimal benchmark for feedback algorithms", *J. Fluid Mech.*, **447**, pp. 179-225.

Carlson, D. R.,Widnall, S. E. and Peeters, M. F., 1982, "A flow-visualization study of transition in plane Poiseuille flow", *J. Fluid Mech.*, **121**, pp. 487-505.

Chang, Y., Collis, S. S. and Ramakrishman, S., 2002, "Viscous effects in control of near-wall turbulence", *Phys. Fluis*, **14** (11), pp. 4069-4080.

Dean, R. D., 1978, "Reynolds number dependence of skin friction and other bulk flow variables in two-dimensional rectangular duct flow", *ASME J. Fluids Eng.*, **100**, pp. 215-222.

Högberg, M., Bewley, T. R. and Henningson, D. S., 2003, "Relaminarization of Re_τ=100 turbulence using gain scheduling and linear state-feedback control", *Phys. Fluis*, **15** (11), pp. 3572-3575.

Iwamoto, K., Suzuki, Y. and Kasagi, N., 2002, "Reynolds number effect on wall turbulence : toward effective feedback control", *Int. J. Heat and Fluid Flow*, **23**, pp. 678-689.

Jiménez, J., 1998, "The largest scales of turbulent wall flows", *CTR Annual Research Briefs*, pp. 137-154.

Kawamura, H., Ohsaka, K., Abe, H. and Yamamoto, K., 1998, "DNS of turbulent heat transfer in channel flow with low to medium-high Prandtl number fluid", *Int. J. Heat and Fluid Flow*, **19**, pp. 482-491.

Kim, J. Moin, P. and Moser, R. D., 1987, "Turbulence statistics in fully developed turbulent channel flow at low Reynolds number", *J. Fluid Mech.*, **177**, pp. 133-166.

Kreplin, H. P. and Eckelmann, H., 1979, "Behavior of the three fluctuating velocity components in the wall region of a turbulent channel flow", *Phys. Fluid*, **22**, pp. 1233-1239.

Kuroda, A., Kasagi, N. and Hirata, M., 1989, "A direct numerical simulation of the fully developed turbulent channel flow", *Proc. Int. Symp. Comput. Fluid Dyn.*, pp. 1174-1179.

Laufer, J., 1951, "Investigation of turbulent flow in a two-dimensional channel", *NACA Rept.*, 1053, pp. 1247-1266.

Liu Z., Adrian R. J. and Hanratty T. J., 2001, "Large-scale modes of turbulent channel flow: transport and structure", *J. Fluid Mech.*, **448**, pp. 53-80.

Moser, R. D., Kim, J. and Mansour, N. N., 1999, "DNS of Turbulent Channel Flow up to Re_τ=590", *Phys. Fluids*, **11**, pp. 943-945.

Niederschulte, M. A., Adrian, R. J. and Hanratty, T. J., 1990, "Measurements of turbulent flow in a channel at low Reynolds numbers", *Experiments in Fluids*, **9**, pp. 222-230.

Patel, V.C. and Head, M.R., 1969, "Some observations on skin friction and velocity profiles in fully developed pipe and channel flows", *J. Fluid Mech.*, **38**, pp. 181-201.

Wygnanski, I.J. and Champagne, F.H., 1973, "On transition in a pipe. Part 1. The origin of puffs and slugs and the flow in a turbulent slug", *J. Fluid Mech.*, **59**, pp. 281-335.

Wygnanski, I., Sokolov, M. and Friedman, D., 1975, "On transition in a pipe. Part 2. The equilibrium puff", *J. Fluid Mech.*, **69**, pp. 283-304.